Kapal: Jurnal Ilmu Pengetahuan dan Teknologi Kelautan
(Kapal: Journal of Marine Science and Technology)
journal homepage : http://ejournal.undip.ac.id/index.php/kapal
2301-9069 (e)
1829-8370 (p)

Experimental and Analytical Investigation of Mooring Angle and Tube Mass Effects on the Dynamic Response of a Submerged Floating Tunnel Segment Model under Wave Excitation

Jamiatul Akmal[1*], Ragil Alvin Dinata[1], Novri Tanti[1], Zulhendri Hasymi[1], Nurcahya Nugraha[1]

[1] Department of Mechanical Engineering, University of Lampung, Lampung 35145, Indonesia
[*] Corresponding Author: jamiatul.akmal@eng.unila.ac.id

Article Info

Keywords:
Submerged Floating Tunnel;
Mooring Cable Inclination;
Damped Forced Vibration;
Hydrodynamic Response;
Experimental Validation

Article history:
Received: 30/08/2025
Last revised: 11/02/2026
Accepted: 04/03/2026
Available online: 04/03/2026
Published: 05/03/2026

DOI:
https://doi.org/10.14710/kapal.v23i1.77442

Abstract

The Submerged Floating Tunnel (SFT) is an alternative infrastructure for crossing transportation routes in deep and wide waters, but further studies are still needed on the dynamic response to wave forces. This study aims to evaluate the dynamic response of a wave-excited Tension Leg type SFT segment model, specifically regarding the influence of the mooring cable angle and the influence of the tube mass. This study was conducted using a damped forced vibration theory approach, exploring the relationship among three main elements of structural dynamics: mass (m), damping (c), and stiffness (k). These parameters are important as fundamental elements that determine the overall stiffness of the structure. The SFT segment model, made of a 3-inch (76 mm) diameter tube with a length of 700 mm, was installed at a depth of 1/6 z below the water surface. The parameters tested included the effect of the mooring cable angle (variations: 15°, 30°, and 45°) and the effect of the tube mass (variations: 0.5 kg, 0.75 kg, and 1 kg). The displacement response of the specimens was obtained from video recordings and analyzed using video tracking software. The experimental results show that an increase in the angle of inclination of the mooring cable leads to an increase in stiffness (k) and a smaller structural displacement. In addition, a larger tube mass results in a greater displacement. The experimental data showed good agreement with the theoretical model of single-degree-of-freedom (SDOF) damped forced vibration, with deviations below 10%. Therefore, this study recommends the use of the largest feasible mooring angle and smallest practical tube mass for optimal SFT design, while still considering real-world application limitations.

1. Introduction

The Submerged Floating Tunnel (SFT) is a novel concept in the field of transportation infrastructure. The concept of SFT involves placing a tubular structure at a specific depth below the water surface, utilizing buoyancy as its carrying capacity [1], as illustrated in Figure 1. Recently, the Submerged Floating Tunnel (SFT) has been discussed as an alternative infrastructure for crossing waterways. These structures are considered more effective, especially for deep and wide straits, where conventional bridges are difficult and expensive to implement [2].

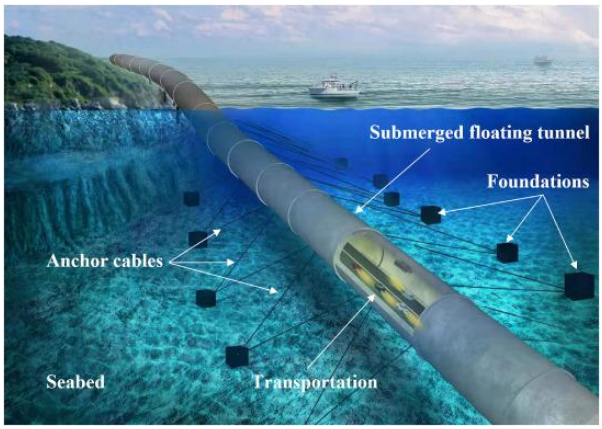

Figure 1. Illustration of the SFT model [3]

Ocean waves are a major challenge in the analysis and design of SFTs [4], especially the influence of hydrodynamic forces caused by ocean waves and currents [5]. These forces are caused by complex interactions between the SFT structural elements and fluid motions [6], which can give rise to vibrations that compromise the stability and safety of the structure [7]. Therefore, a fundamental understanding of the dynamic behaviour of SFTs under the influence of wave forces is important as a basis for their design.

Several previous researchers have conducted studies on the dynamic behaviour of Submerged Floating Tunnel (SFT), either analytically, numerically, or experimentally [8]. Analytical studies focus on exploring mathematical models of the structure's dynamic response [9], [10], while numerical approaches use computer simulations to analyse fluid-structure interactions in a more complex manner [11], [12]. Numerical studies conducted by [13] and [14], for example, evaluate the influence of mooring cable layout on the hydrodynamic response of SFTs, including the effects of hydroelasticity and fluid–structure interaction. However, analytical approaches are generally carried out with simplifying assumptions on design variables, so they do not fully represent the real conditions in the field. On the other hand, the more realistic numerical approach relies heavily on the validation of experimental data as the basis for its justification. The main issue that arises is the limited experimental data available, especially those that specifically evaluate the influence of key design parameters such as mooring line inclination angle and structural mass variation on the dynamic response of SFTs [15]. This creates a research gap in understanding the direct contribution of these two parameters to the stability and dynamic efficiency of the structure.

In contrast to previous studies, this research aims to fill the gap by presenting a controlled experimental approach that systematically evaluates the effects of mooring cable angle and tube mass on displacement response, and validates it through a theoretical model of a one-degree-of-freedom system with forced damping. The novelty of this study lies in the integration of experimental methods and analytical approaches to define key parameter relationships, namely mass (m), damping factor (c), and stiffness (k). This research is important to understand the basic parameters useful in designing SFTs subjected to wave-induced loads, in order to obtain an optimal design to improve stability, efficiency, and dynamic reliability [16].

The damping factor c is determined experimentally by the Logarithmic Decrement Method, which measures the logarithmic decrement rate of amplitude over time [17]. Meanwhile, stiffness (k) is equivalently calculated based on the mooring line configuration. The equivalent horizontal stiffness can be determined based on the balance of forces induced by the mooring line, depending on its slope, elasticity value, initial length, and cross-sectional area. This approach is known as the beam on elastic foundation model [18], which linearly represents the stiffness of the structure in the horizontal direction.

This research has significance as a theoretical validation of the basic elements of dynamic analysis in segment models. Furthermore, the research on segment models can be bridged into continuous models with various numerical theories, such as the Direct Integration - Mode Superposition Method (DI-MSM), which was recently developed for the dynamic analysis of large-dimensional continuous structures [19]. This approach opens up opportunities to develop a more accurate and efficient numerical simulation framework in designing SFTs, considering real sea conditions and technical configuration variations. Thus, this research not only contributes to the strengthening of fundamental aspects of dynamic analysis but also provides a new direction in the development of experimentally and numerically based predictive methods for next-generation subsea structures. However, it must be acknowledged that research conducted on a laboratory scale is still relatively simple and cannot fully describe the behavior of SFTs in the real world. Therefore, further research is needed with variables that approximate field conditions, involving large-scale prototypes, irregular wave motion, ocean currents, and complex mooring cable configurations to gain a comprehensive understanding of the actual performance of SFTs.

2. Method

2.1. Develop a model and an Analytical Solution

The structure consists of the SFT model segment and reference coordinates in this study, as shown in Figure 2. The reciprocating motion of the wave generator creates waves that provide periodic excitation forces to the structure, as demonstrated in our previous research [20]. The total water depth in the test medium is 0.6 m, and the SFT is positioned 0.1 m below the water surface. A 3-inch (7.62 cm) diameter tube is held by a mooring cable configuration at an angle θ to the vertical line. Cartesian coordinates are used as a reference to monitor $x, \dot{x},$ and $\ddot{x}$ which represent displacement, velocity, and acceleration, respectively. The observed parameters are the effects of the mooring cable angle and tube mass on the vibration response subjected to the wave excitation force F(t).

Vibrations in the system can be analysed using an equivalent model as shown in Figure 3, where m is the mass of the tube (kg), c is the damping factor (N.s/m), and k is the spring stiffness (N/m). The spring element k represents the total horizontal stiffness, which is calculated based on the tension and configuration of the mooring cables. Meanwhile, the damping factor c is evaluated as viscous damping resulting from fluid-structure interaction.

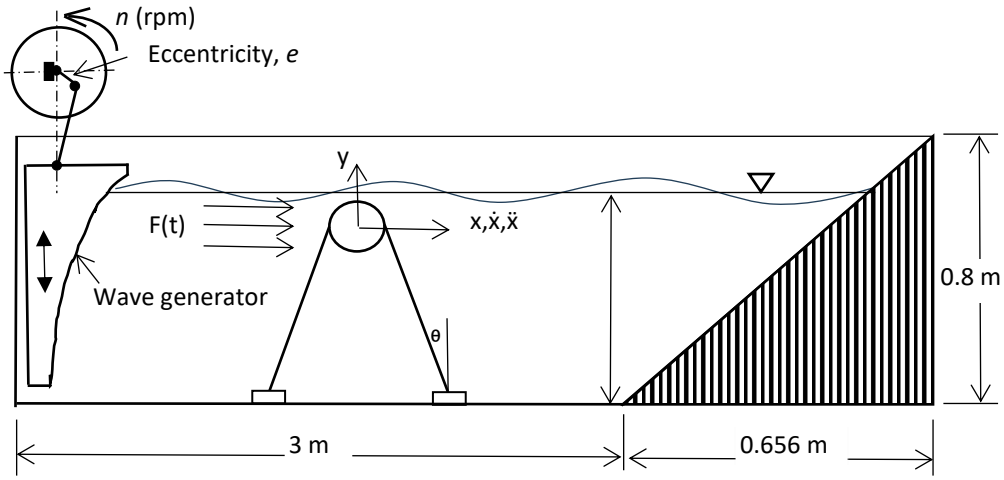

Figure 2. The SFT model with parameters and reference coordinates.

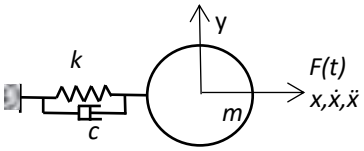

Figure 3. An equivalent model of a forced vibration system with a SDOF.

The vibration equation for Figure 3 is a damped forced vibration that can be written as a second-order differential equation, as shown in Eq. (1). The general solution given in Eq. (2) consists of two components: the transient response and the steady-state response. The transient component (first term) decays over time due to the effect of damping, while the steady-state component (second term) is a harmonic oscillation with a certain amplitude, determined by the excitation frequency.

$$m\ddot{x} + c\dot{x} + kx = Fo \sin \omega t \tag{1}$$

$$x(t) = X_0 e^{-\zeta \omega_n t} \sin(\omega_d t + \phi_0) + \frac{F_0}{\sqrt{(k - m\omega^2)^2 + (c\omega)^2}} \sin(\omega t - \phi) \tag{2}$$

$$\phi = tan^{-1}\left(\frac{c\omega}{k - m\omega}\right) \tag{3}$$

In Eq. (2), $x(t)$ is the displacement of the system as a function of time (m), X_0 is the initial amplitude of the transient response (m), $e^{-\zeta \omega_n t}$ is the non-dimensional exponential factor that represents the damping effect of the system as a function of time. Here, ζ is the damping ratio (unitless), ω_n is the natural frequency of the undamped system (rad/s), ω_d is the damped natural frequency (rad/s), and ϕ_0 is the initial phase of the transient response (rad). Furthermore, F_0 is the amplitude of the external force acting on the system (N), ω is the frequency of the external force acting on the system (rad/s), and ϕ is the phase shift caused by the external force (rad), whose value can be calculated using Eq. (3), where all symbols follow standard vibration theory notation.

2.1.1. Horizontal Stiffness

The stiffness of the SFT increases with the presence of mooring cables characterized by the vertical axis angle (θ), initial tension (T_0), length (L), elastic modulus (E), and cross-sectional area (A), as shown in Figure 4. The vertical stiffness and horizontal stiffness of the mooring system equation can be calculated using Eq. (4), and the tension of the mooring cable T_0 can be calculated using Eq. (5).

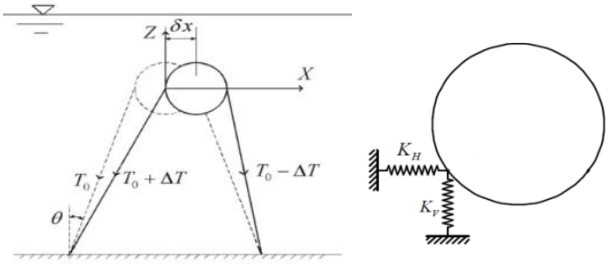

Figure 4. Stiffness model of the SFT [19].

$$K_v = \frac{2T_0}{L_t}, \qquad K_h = \frac{2EA}{L_t} sin^2\theta \tag{4}$$

$$T_0 = \frac{F/4}{\cos\theta}, \; F = F_b - F_w \tag{5}$$

2.1.2. Hydrodynamic Force

The hydrodynamic force of waves on tubular structures is described by the Morison equation, which consists of inertial and drag forces combined linearly [21]. The maximum hydrodynamic force occurs near the water surface and decreases with increasing distance. The Morison equation can be seen in Eq. (6) [22], where ρ is the density of water, C_D is the drag coefficient, C_M is the inertia coefficient, u is the horizontal velocity of water, du/dt is the horizontal acceleration of water, and D is the diameter of the tube.

$$F = \frac{1}{2}\rho C_D u|u| + \rho C_M \frac{\pi D^2}{4}\frac{du}{dt} \tag{6}$$

2.1.3. Viscous damping coefficient and structural damping

The damping coefficient is determined using the Logarithmic Decrement Method [23]. The method involves applying an initial displacement to the model structure and recording its response. The logarithmic decrement (δ) is defined in Eq. (7).

$$\delta = \frac{1}{n} ln \frac{X_0}{X_n} \tag{7}$$

where X_0 is the initial amplitude, X_n is the amplitude after nnn cycles, and n is the number of oscillation cycles considered. Once δ is obtained, the damping ratio (ζ) can be calculated using Eq. (8). If the damping ratio is known, the damping coefficient (C) is determined using Eq. (9), where the critical damping coefficient c_c and the natural frequency ω_n are expressed in Eq. (10) and (11), respectively.

$$\zeta = \frac{\delta}{\sqrt{(2\pi)^2 + \delta^2}} \tag{8}$$

$$C = \zeta \cdot c_c \tag{9}$$

$$c_c = 2m\omega_n \tag{10}$$

$$\omega_n = \sqrt{\frac{k}{m}} \tag{11}$$

2.2. Experimental Study

Referring to Figure 2, the eccentricity was set at 2 cm from the rotor axis, and the eccentric rotor mechanism was operating at a speed of 110 rpm. To maintain wave consistency, each data collection starts at the 5th second (to achieve a stable state) and lasts for 12 seconds, which is sufficiently short to minimize the influence of reflected waves. The generated wave is classified as a Stokes wave with an amplitude of 2.99 cm, a wavelength of 51.98 cm, a period of 0.544 s, and a wave height of 5.98 cm. The experimental test setup in this study is shown in Figure 5, and the specifications of the generated wave can be seen in Table 1, while the research parameters are shown in Table 2.

Table 1. The specifications of the generated wave

No	Parameter	Symbol	Unit	Value
1	Wavelength	λ	m	0.5198

2	Amplitude	*A*	m	0.0299
3	Period	*T*	s	0.544
4	Wave height	*H*	m	0.0598

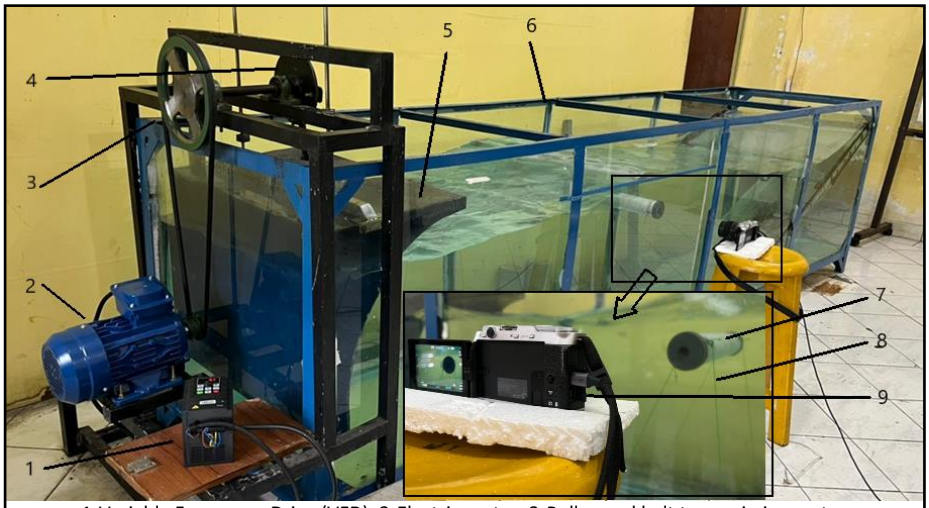

1-Variable Frequency Drive (VFD), 2-Electric motor, 3-Pulley and belt transmission system, 4-eccentric mechanism, 5-flap generator, 6-Water Tank, 7-SFT Segment Model, 8-Mooring cables, and 9-Digital camera

Figure 5. Experimental test setup for the SFT model.

Table 2. The research parameters

No	Parameter	Symbol	Unit	Value
1	Cylinder Diameter	*D*	m	0.076
2	Mass	*m*	kg	0.5
				0.75
				1
3	Mooring cable inclination angle	θ	degree	15
				30
				45
4	Tube position depth	z	m	0.1

The movement of the SFT structure model is identified using video recordings taken with a digital camera pointed at the test object. The video recordings are then processed using video analysis tracking software to identify the position of the object at any given time relative to a specified reference point [24], [25]. The camera used for motion capture was a Fujifilm X-T200 (APS-C CMOS, 24.2 MP), with an XC 15-45 mm f/3.5-5.6 OIS lens. Video was recorded at Full HD 1080p resolution with a frame rate of 30 fps to ensure position tracking accuracy in the tracking software. Before testing, calibration is performed using a calibration stick to ensure that pixel coordinates correspond to actual dimensions. The auto-tracker is the final step in the tracking software, used to determine the position of the object's points and visualize them as a displacement graph over time. Figure 6 shows the raw tracking graph, colored red, which represents the position of the object in real time. A more stable graph, colored black, is obtained after reducing the recording noise. This graph is then exported and used to determine the dominant frequency through Fast Fourier Transform (FFT) and evaluation of the damped vibration characteristics.

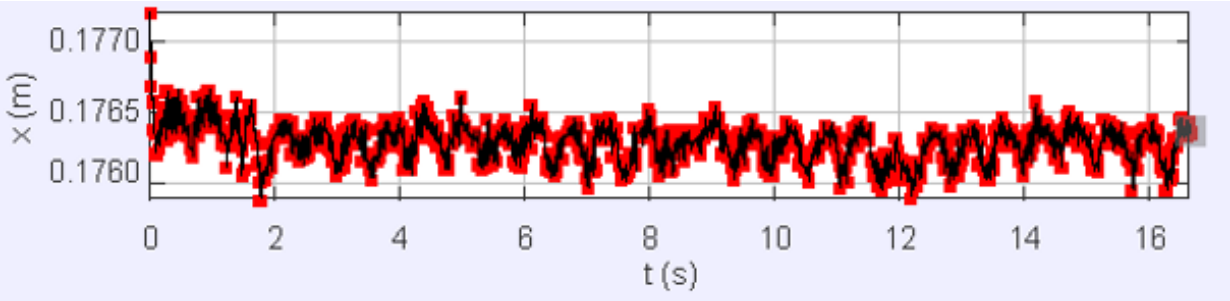

Figure 6. Results of tracking the movement of the SFT model using Tracker software.

3. Results and Discussion

Figure 7 shows a damped oscillation graph obtained from a damped free vibration test, in which the SFT model was given an initial displacement X_0 and then suddenly released. The movement of the model was recorded on video and converted into a displacement graph using video tracking software. It can be seen that the displacement amplitude gradually

decreases over time. This pattern is consistent with the characteristics of damped vibration, where the oscillation energy gradually decreases due to the interaction between the structure and the fluid [26]. The peak amplitudes x_1, x_2, ... of this graph are then used in the logarithmic decrement method to determine the damping ratio. The rate of amplitude decrease is presented in Table 3.

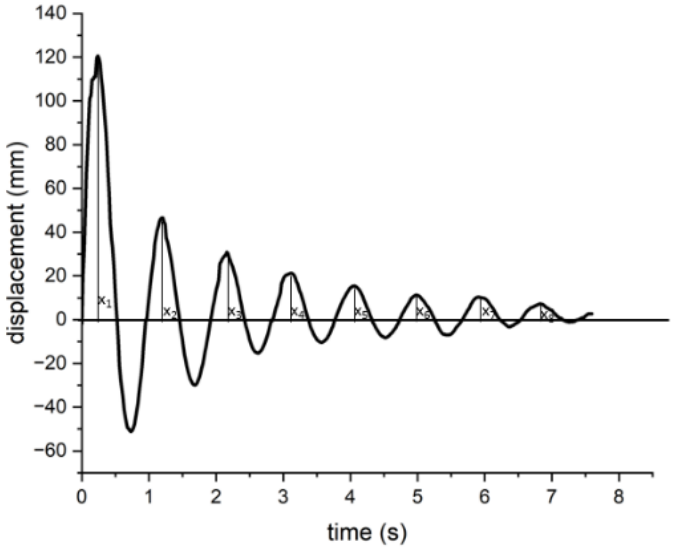

Figure 7. The damped oscillation graph.

Table 3. The rate of amplitude reduction.

Peak Number	Time (s)	Amplitude (mm)
1	0.3	120
2	1.0	75
3	1.7	50
4	2.3	35
5	3.0	25
6	3.7	18
7	4.3	13
8	5.0	10

Using the Logarithmic Decrement Method for the first five peaks, the logarithmic decrement (δ) and the damping ratio (ζ) were obtained as follows:

$$\delta = \frac{1}{n5} ln \frac{120}{18} = 0.38 \quad (12)$$

$$\zeta = \frac{\delta}{\sqrt{(2\pi)^2 + \delta^2}} = 0.06 \quad (13)$$

The value of the damping coefficient (C) can vary due to the influence of mass and structural stiffness, resulting in different natural frequencies. The complete dynamic response for each parameter is presented in Table 4, which presents the displacement amplitude of the SFT structure, derived from the maximum and minimum values corresponding to each variation in mooring angle and tube mass. All experiments were conducted over 12 seconds.

Table 4. Experimental parameters and their dynamic responses

Mass, m (kg)	Mooring Cable Angle, θ (degres)	Wave Force, $F(t)$ (N)	Damping coefficient, C (N.s/m)	Amplitude, A (mm)
0.5	15	0.71	0.427	14.9
	30	0.71	2.409	8
	45	0.71	3.239	1.7
0.75	15	0.71	0.341	22.9
	30	0.71	0.921	13.1
	45	0.71	1.748	2.6
1	15	0.71	0.279	49.3
	30	0.71	0.797	27.1

45	0.71	1.064	5.7

3.1. Effect of Mooring Cable Angle on Displacement

Figure 8 shows the displacement of a 0.5 kg SFT model. The graph compares three mooring cable angles: 15°, 30°, and 45°. The results are clear: larger mooring angles result in smaller displacements, while smaller angles result in larger structural movements. The displacement response is influenced by the effective horizontal stiffness contributed by the inclined mooring cables. This behavior is consistent with previous numerical and analytical studies, which reported that more inclined mooring configurations increase the restoring force and suppress excessive movement of the SFT structure under wave loading [27].

FFT analysis supports this trend, showing a frequency of 1.6 Hz from the experiment and 1.8 Hz from the analytical calculations. Although the peak and dominant frequencies of the FFT results do not quantitatively coincide, they show a consistent trend in displacement as the mooring angle changes. This consistency indicates that in the analytical SDOF model, the system response depends on variations in stiffness and natural frequency. Similar observations were reported by [28], [16], where numerical models successfully reproduced frequency trends but showed deviations in spectral amplitudes when compared to experiments or more comprehensive simulations.

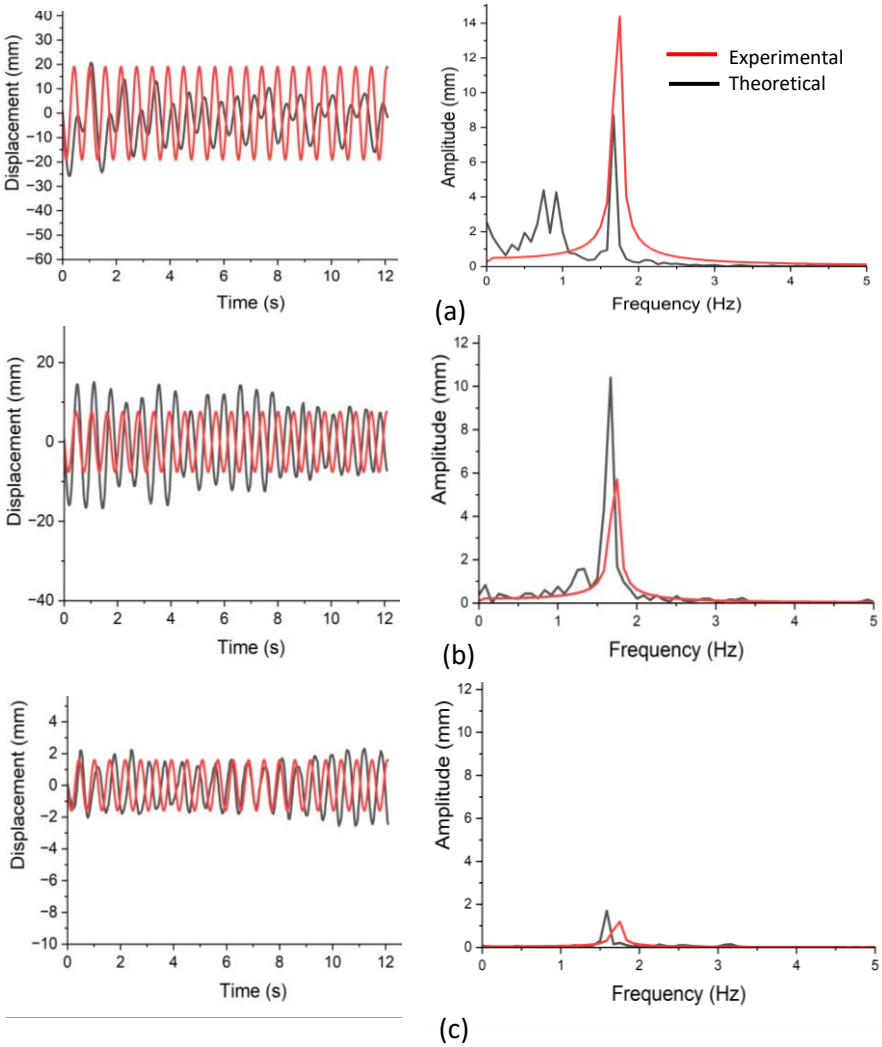

Figure 8. The displacement of the SFT model with a mass of 0.5 kg. (a) 15° angle, (b) 30° angle, (c) 45° angle.

The quantitative differences between the experimental and theoretical FFT results can be attributed to several factors. First, the analytical model adopts idealized assumptions, including linear stiffness, uniform damping, and simplified hydrodynamic loading based on Morison's formulation. In contrast, the experimental system is affected by nonlinear hydrodynamic effects, wave reflections from the tank boundary, turbulence, additional viscous damping, and local friction at the mooring joints. These effects are known to broaden spectral peaks and reduce peak sharpness in the experimental FFT results, as discussed in hydrodynamic studies of SFT under wave influence [29], [30]. Second, the interactions between the fluid and the structure, explicitly considered in the numerical model but ignored in the simplified analytical formulation, also contribute to differences in amplitude and frequency resolution.

Therefore, the agreement between the experimental and theoretical results in this study should be interpreted in terms of consistency in trends and dominant frequency behavior, rather than exact numerical similarity. The combined use of time-domain displacement history and FFT analysis provides a more comprehensive understanding of the SFT dynamic response, where the time-domain plots emphasize amplitude attenuation and damping effects, while the frequency-domain results highlight stiffness-driven frequency shifts. This interpretation aligns with established vibration theory and recent SFT research, which confirms that increasing the mooring cable angle is an effective strategy for reducing displacement response and enhancing dynamic stability. These findings provide useful guidance for SFT design, particularly in selecting appropriate mooring angles to improve structural stability and minimize unwanted vibrations.

3.2. Effect of Tube Mass on Displacement

Figure 9 shows the displacement response and FFT results of the SFT model at a mooring angle of 15°, with variations in tube mass of 0.5 kg, 0.75 kg, and 1 kg. The displacement graph (left) indicates that as the tube mass increases, the amplitude of the resulting oscillations also increases. Meanwhile, the FFT analysis (right) shows that the dominant frequency of the experimental results has good agreement with the theoretical predictions, in the sense that both exhibit the same trend and peak-shift behavior as mass increases, even though the numerical values are not identical. Quantitative deviations are caused by theoretical models that assume ideal conditions, such as perfect rigidity, uniform damping, and linear hydrodynamic force, while the experiment is affected by additional factors, including fluid turbulence, small asymmetries in cable tension, friction at the supports, and camera-tracking noise. These results confirm that mass has a significant influence on both the amplitude and frequency response of the SFT system.

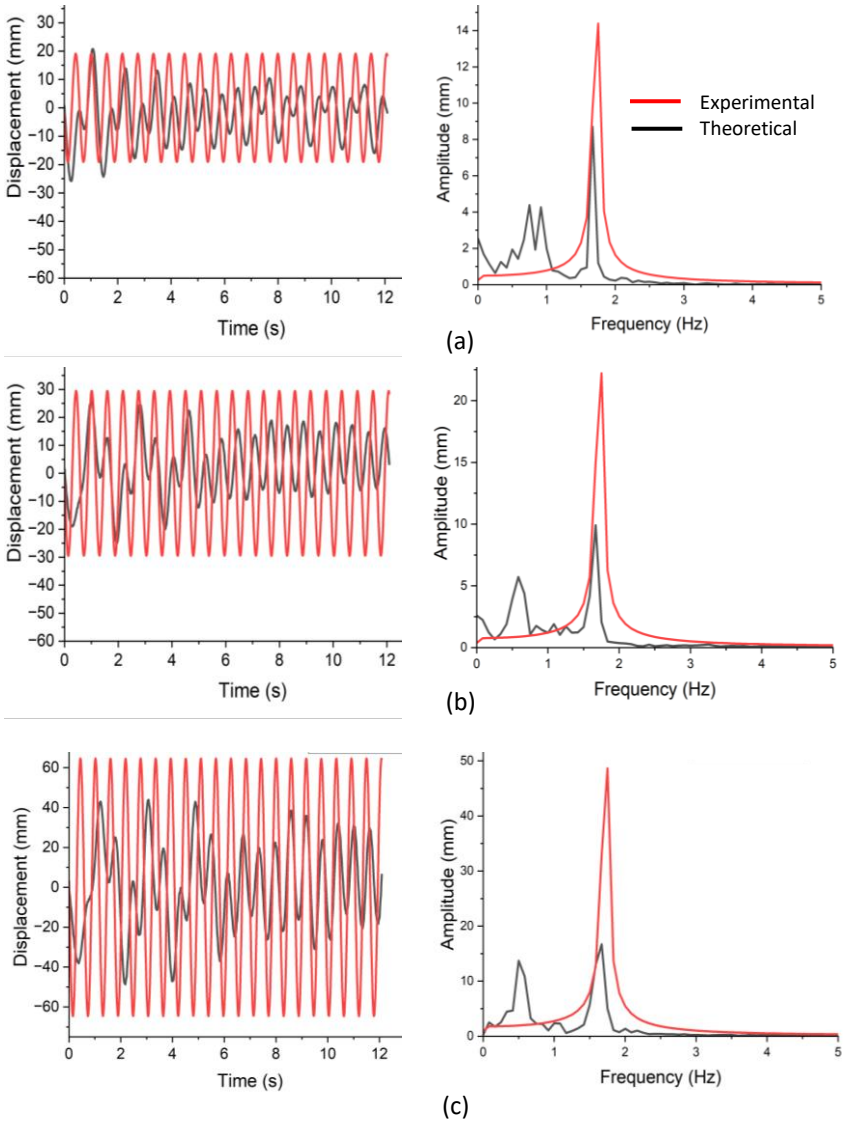

Figure 9. The displacement response and FFT results of the SFT model at a mooring angle of 15°, with variations in tube mass of (a) 0.5 kg, (b) 0.75 kg, and (c) 1 kg.

In a forced damped SDOF model, the steady-state amplitude $|X|$ depends on $|k - m\omega^2|$ and $c\omega$. An increase in mass can lower the natural frequency $\left(\omega_n = \sqrt{k/m}\right)$, shifting the system closer to or further from the excitation frequency of the wave, so that the amplitude can increase if the shift brings the conditions closer to resonance. Several SFT studies report strong

sensitivity to mass and hydrodynamic parameters [31], [32]. Physical model tests and numerical simulations show that changes in mass/configuration can alter the FFT peak and displacement magnitude, with good agreement between experimental data and theoretical predictions when wave forces are modelled using the Morison equation. Larger mass produces greater displacement at certain frequency combinations, which can be explained by the ω_n shift approaching the excitation ω, thereby amplifying the response. The findings of this study offer valuable input for SFT design, emphasizing the importance of reducing structural mass without neglecting the limitations imposed by field conditions.

Figure 10 shows the average amplitude graph, comparing the experimental results with the analytical predictions. From the graph, it can be seen that as the mass of the tube increases, the displacement also tends to increase, especially at small angles (15°) where the structural response is greatest. Conversely, at larger angles (30° and 45°), the displacement amplitude is significantly smaller because the inclined mooring line configuration provides additional stiffness in the horizontal direction. In general, the experimental and theoretical results show good agreement, although at a mass of 1 kg and an angle of 15°, there is a larger discrepancy. This is likely due to additional hydrodynamic effects, nonlinear effects not modelled in the mooring system, or uncertainties in the experimental measurements.

This finding is consistent with previous research by [33], which showed that mass variation has a significant effect on the natural frequency shift of SFTs and can either strengthen or weaken the resonance effect depending on the wave frequency. Additionally, [34] emphasise that the configuration and inclination of mooring cables can affect structural stiffness and amplitude. Similar findings were reported by [35], who discovered that mass variations influence buoyancy forces, which in turn affect cable tension and horizontal stiffness. Thus, the results of this study not only support previous analytical and numerical models but also provide experimental validation that increasing the mooring cable angle and using a smaller structural mass are effective in reducing displacement amplitude. Practically, these findings can serve as a basis for designing SFTs to be more stable, efficient, and safe when operating in real-world water conditions.

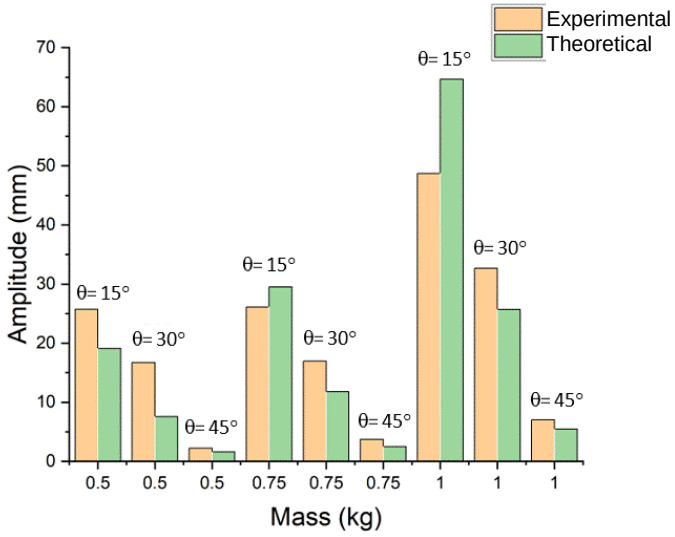

Figure 10. Average amplitude graph: experimental and analytical results.

4. Conclusion

This study examines the dynamic response of a tension-leg Submerged Floating Tunnel (SFT) segment model subjected to wave excitation, focusing on the effect of mooring cable inclination angle and variations in tube mass on structural displacement. Based on experimental testing and theoretical analysis using a SDOF vibration model, it was found that increasing the mooring cable inclination angle consistently increases the effective stiffness of the system, thereby reducing the displacement amplitude. Conversely, increasing tube mass tends to increase the displacement response due to increased system inertia effects.

Time domain analysis reveals quantitative discrepancies between the experimental results and theoretical calculations, particularly in displacement amplitude. However, frequency domain analysis using the Fast Fourier Transform (FFT) demonstrates a consistent trend in the dominant frequency changes, indicating that the system's primary dynamic mechanisms are well represented by the analytical model used. These quantitative discrepancies are influenced by the limitations of the theoretical model's idealized assumptions, as well as by nonlinear effects in the experimental testing, such as wave reflection, fluid turbulence, additional damping, and local friction in the mooring cable system.

Overall, the results of this study confirm that the inclination angle of the mooring cable and the mass of the structure are key design parameters that significantly affect the dynamic stability of the SFT segment. These findings provide an important contribution in the form of experimental data as a basis for validating analytical and numerical models, and can be used as an initial reference in SFT design to minimize displacement response and avoid potential resonance, while still considering the limitations of field conditions and test scales.

Acknowledgements

The authors would like to express their sincere gratitude to the Structural Mechanics Laboratory, Faculty of Engineering, University of Lampung, for providing the necessary facilities and support throughout this research. Their assistance and resources were invaluable in conducting the experiments and obtaining the results presented in this study.

References

[1] G. A. Torres-Alves, C. M. P. 'T Hart, O. Morales-Nápoles, and S. N. Jonkman, "Structural reliability analysis of a submerged floating tunnel under copula-based traffic load simulations," *Engineering Structures*, vol. 269, p. 114752, Oct. 2022, doi: https://doi.org/10.1016/j.engstruct.2022.114752.

[2] M.-C. Tang, "Forms and Aesthetics of Bridges," *Engineering*, vol. 4, no. 2, pp. 267–276, Apr. 2018, doi: https://doi.org/10.1016/j.eng.2017.12.013.

[3] N. Fan, J. Jiang, L. Guo, H. Lin, and L. Wang, "Numerical analysis of partial impact forces of offshore submerged floating tunnel encountered submarine slide hazards," *Ocean Engineering*, vol. 266, p. 112903, Dec. 2022, doi: https://doi.org/10.1016/j.oceaneng.2022.112903.

[4] Y. Xiang and Y. Yang, "Challenge in Design and Construction of Submerged Floating Tunnel and State-of-art," *Procedia Engineering*, vol. 166, pp. 53–60, 2016, doi: https://doi.org/10.1016/j.proeng.2016.11.562.

[5] Z. Yang et al., "Experimental study on the wave-induced dynamic response and hydrodynamic characteristics of a submerged floating tunnel with elastically truncated boundary condition," *Marine Structures*, vol. 88, p. 103339, Mar. 2023, doi: https://doi.org/10.1016/j.marstruc.2022.103339.

[6] H. Peng, J. Guo, H. Ping, Y. Sun, G. Liu, and G. Liu, "Numerical analysis of the fluid–structure interaction characteristics of a pontoon submerged floating tunnel," *Ocean Engineering*, vol. 301, p. 117660, Jun. 2024, doi: https://doi.org/10.1016/j.oceaneng.2024.117660.

[7] D. Shao, J. Zheng, J. Zhang, Y. Yang, and J. Zhang, "Vibrating behavior of submerged floating tunnel in current field investigated with hybrid vector-autoregressive model," *Ocean Engineering*, vol. 256, p. 111359, Jul. 2022, doi: https://doi.org/10.1016/j.oceaneng.2022.111359.

[8] G. Iovane, F. M. Mazzolani, R. Landolfo, E. Begovic, E. Bilotta, and B. Faggiano, "Assessment of experimental tests on SFT small scale specimen," *Applied Ocean Research*, vol. 138, p. 103656, Sep. 2023, doi: https://doi.org/10.1016/j.apor.2023.103656.

[9] J. Xie and J. Chen, "Dynamic response analysis of submerged floating tunnel - canyon water system under earthquakes," *Applied Mathematical Modelling*, vol. 94, pp. 757–779, Jun. 2021, doi: https://doi.org/10.1016/j.apm.2021.01.031.

[10] J. Hou et al., "Analysis of the dynamic response of submerged floating tunnels to wave-induced loads, incorporating joint mechanical properties," *Ocean Engineering*, vol. 297, p. 117079, Apr. 2024, doi: https://doi.org/10.1016/j.oceaneng.2024.117079.

[11] A. Gilmanov, T. B. Le, and F. Sotiropoulos, "A numerical approach for simulating fluid structure interaction of flexible thin shells undergoing arbitrarily large deformations in complex domains," *Journal of Computational Physics*, vol. 300, pp. 814–843, Nov. 2015, doi: https://doi.org/10.1016/j.jcp.2015.08.008.

[12] W. Chul Chung, C. Jin, M. Kim, and J. Hwang, "Comparison Study and Forensic Analysis between Experiment and Coupled Dynamics Simulation for Submerged Floating Tunnel Segment with Free Ends under Wave Excitations," *Computer Modeling in Engineering & Sciences*, vol. 137, no. 1, pp. 155–174, 2023, doi: https://doi.org/10.32604/cmes.2023.026754.

[13] X. Yuan, J. Liu, J. Zhou, and A. Guo, "Effect of cable layout on hydrodynamic response of submerged floating tunnel under wave action," *Ocean Engineering*, vol. 280, p. 114257, Jul. 2023, doi: https://doi.org/10.1016/j.oceaneng.2023.114257.

[14] X. Ye, X. Zhou, M. Wang, D. Qiao, X. Zhao, and L. Wang, "Global Responses Analysis of Submerged Floating Tunnel Considering Hydroelasticity Effects," *Journal of Marine Science and Engineering*, vol. 12, no. 10, p. 1854, Oct. 2024, doi: https://doi.org/10.3390/jmse12101854.

[15] H. Ding et al., "Analysis of the influence of key structural parameters on the dynamic response of oval cross-section SFT under wave-current action," *Ocean Engineering*, vol. 336, p. 121738, Sep. 2025, doi: https://doi.org/10.1016/j.oceaneng.2025.121738.

[16] W. Pan, C. Cui, C. Chen, M. Xie, Q. Gu, and Z. Yang, "Optimization Analysis of the Arrangement of the Submerged Floating Tunnel Subjected to Waves," *Journal of Marine Science and Engineering*, vol. 12, no. 5, p. 764, Apr. 2024, doi: https://doi.org/10.3390/jmse12050764.

[17] C. Li et al., "Experimental study on dynamic response of submerged floating tunnel moored with different material cables," *Ocean Engineering*, vol. 329, p. 121127, Jun. 2025, doi: https://doi.org/10.1016/j.oceaneng.2025.121127.

[18] M. Sato, S. Kanie, and T. Mikami, "Mathematical analogy of a beam on elastic supports as a beam on elastic foundation," *Applied Mathematical Modelling*, vol. 32, no. 5, pp. 688–699, May 2008, doi: https://doi.org/10.1016/j.apm.2007.02.002.

[19] J. Akmal, N. Nugraha, and A. Lubis, "Direct Integration Mode Superposition: A Simple Method for Dynamic Analysis of Submerged Floating Tunnel (SFT)," *Journal of Mechanical Engineering*, vol. 22, no. 1, 2025. [Online]. Available: https://search.ebscohost.com/

[20] J. Akmal, "Dynamic response of Tension Leg Platform (TLP): A comparative study between circular and square pontoon usage (in Indonesian)," *Machine*, vol. 8, no. 1, pp. 45–50, Apr. 2022, doi: https://doi.org/10.33019/jm.v8i1.2928.

[21] J. Akmal et al., "Hydrodynamic forces on submerged floating tube: The effect of curvature radius and depth level," *Kapal: Jurnal Ilmu Pengetahuan dan Teknologi Kelautan*, vol. 19, no. 1, pp. 1–8, Feb. 2022, doi: https://doi.org/10.14710/kapal.v19i1.44019.

[22] H. Ding, B. Huang, L. Cheng, K. Li, and Q. Ren, "Hydrodynamic experiment of submerged floating tunnel under regular wave and current actions during construction period," *Marine Structures*, vol. 93, p. 103508, Jan. 2024, doi: https://doi.org/10.1016/j.marstruc.2023.103508.

[23] L. Flis, G. Szwoch, and P. Krawczyk, "Determining a damping coefficient by using a microelectromechanical systems accelerometer for finite element method simulation purposes on a discrete damper example," *Advances in Science and Technology Research Journal*, vol. 19, no. 6, pp. 275–290, Jun. 2025, doi: https://doi.org/10.12913/22998624/202753.

[24] R. Kaushik, S. C. Swami, D. Sharma, and P. Ahluwalia, "Object Detection and Tracking in Real Time Video," *International Journal of Pharmaceutical Research*, pp. 56490–56493, May 2020, doi: https://doi.org/10.61841/V24I5/400264.

[25] S. Abba, A. M. Bizi, J.-A. Lee, S. Bakouri, and M. L. Crespo, "Real-time object detection, tracking, and monitoring framework for security surveillance systems," *Heliyon*, vol. 10, no. 15, p. e34922, Aug. 2024, doi: https://doi.org/10.1016/j.heliyon.2024.e34922.

[26] Md. M. Alam, "New scaling of critical damping and reduced frequency for mechanically excited systems," *Shock and Vibration*, vol. 59, no. 2, p. 2600, Mar. 2025, doi: https://doi.org/10.59400/sv2600.

[27] K. Jeong, S. Min, M. Jang, D. Won, and S. Kim, "Feasibility study of submerged floating tunnels with vertical and inclined combined tethers," *Ocean Engineering*, vol. 265, p. 112587, Dec. 2022, doi: https://doi.org/10.1016/j.oceaneng.2022.112587.

[28] X. Ye, X. Zhou, M. Wang, D. Qiao, X. Zhao, and L. Wang, "Global Responses Analysis of Submerged Floating Tunnel Considering Hydroelasticity Effects," *Journal of Marine Science and Engineering*, vol. 12, no. 10, p. 1854, Oct. 2024, doi: https://doi.org/10.3390/jmse12101854.

[29] D. Won, J. Seo, S. Kim, and W.-S. Park, "Hydrodynamic Behavior of Submerged Floating Tunnels with Suspension Cables and Towers under Irregular Waves," *Applied Sciences*, vol. 9, no. 24, p. 5494, Dec. 2019, doi: https://doi.org/10.3390/app9245494.

[30] K. Jeong, J. Kim, S. Min, H. Shin, and S. Kim, "Design strategy for submerged floating tunnels: Structural response analysis and rational mooring-boundary condition combinations under wave loads," *Ocean Engineering*, vol. 317, p. 120097, Feb. 2025, doi: https://doi.org/10.1016/j.oceaneng.2024.120097.

[31] Z. Liu, X. Shi, T. Guo, H. Ren, and M. Zhang, "Investigation on hydrodynamic response and characteristics of a submerged floating tunnel based on hydrodynamic tests," *Ocean Engineering*, vol. 300, p. 117187, May 2024, doi: https://doi.org/10.1016/j.oceaneng.2024.117187.

[32] W. Pan, M. He, and C. Cui, "Experimental Study on Hydrodynamic Characteristics of a Submerged Floating Tunnel under Freak Waves (I: Time-Domain Study)," *Journal of Marine Science and Engineering*, vol. 11, no. 5, p. 977, May 2023, doi: https://doi.org/10.3390/jmse11050977.

[33] G. Guo, S. Zhong, Q. Zhang, J. Zhong, and D. Liu, "Effect of Additional Mass on Natural Frequencies of Weight-Sensing Structures," *Sensors*, vol. 23, no. 17, p. 7585, Sep. 2023, doi: https://doi.org/10.3390/s23177585.

[34] G. A. Amaral, C. P. Pesce, and G. R. Franzini, "Mooring system stiffness: A six-degree-of-freedom closed-form analytical formulation," *Marine Structures*, vol. 84, p. 103189, Jul. 2022, doi: https://doi.org/10.1016/j.marstruc.2022.103189.

[35] F. Foti, L. Martinelli, E. Morleo, and F. Perotti, "Dynamic response of Submerged Floating Tunnels: An enhanced semi-analytical approach," *Ocean Engineering*, vol. 294, p. 116648, Feb. 2024, doi: https://doi.org/10.1016/j.oceaneng.2023.116648